Desalination and Water Treatment
www.deswater.com
doi: 10.5004/dwt.2020.25039

179 (2020) 183–196
March

Adsorption potential of zirconium-ferrite nanoparticles for phenol, 2-chlorophenol and 2-nitrophenol: thermodynamic and kinetic studies

Shah Raj Ali[a], Mahesh Chandra Arya[a], Abul Kalam[b], Abdullah G. Al-Sehemi[c], Zenab Khan[a], Sadaf Ansari[a], Rajesh Kumar[a,*]

[a]*Department of Chemistry, Kumaun University, Nainital 263002, Uttarakhand, India, Tel. +91-9458115534; email: drkumarntl@gmail.com*
[b]*Department of Chemistry, King Khalid University, Abha 61413, Saudi Arabia*
[c]*Research Centre for Advanced Materials Science, King Khalid University, Abha 61413, Saudi Arabia*

Received 23 May 2019; Accepted 14 October 2019

ABSTRACT

Adsorption of phenol, 2-chlorophenol and 2-nitrophenol on zirconium-ferrite nanoparticles, has been studied. Zirconium-ferrite nanoparticles were synthesized using a reported method and characterized using different analytical techniques, such as, X-ray diffraction pattern, BET surface area analysis, scanning electron microscopy-energy dispersive X-ray spectroscopy, transmission electron microscopy, thermal gravimetric analysis, zeta potential analysis, Fourier transform infrared spectroscopy and Raman spectral studies. It was found to be associated with improved nanofeatures in terms of high surface area (392 m^2/g) and less pore volume (0.1723 cm^3/g). The synthesized material showed high adsorption affinity towards all three phenols. The adsorption data were found to follow Langmuir adsorption isotherm with the square of the regression coefficient (R^2) 0.994, 0.995 and 0.995 for phenol, 2-chlorophenol and 2-nitrophenol, respectively, at 288 K. The adsorption capacity of zirconium-ferrite nanoparticles was found to be 334.44, 354.61 and 375.93 mg/g for phenol, 2-chlorophenol and 2-nitrophenol, respectively, under the optimized conditions, namely, pH, contact time, concentration of adsorbate, amount of adsorbent and temperature. The thermodynamic parameter, namely, change in Gibbs free energy ($\Delta G°$), enthalpy ($\Delta H°$) and entropy ($\Delta S°$) have been determined by conducting the adsorption experiments at 288, 303, 318 and 333 K. The values of $\Delta G°$, $\Delta H°$ and $\Delta S°$ were found to be negative which showed that the adsorption was unfavorable by $\Delta S°$ but highly favorable by $\Delta H°$ and the spontaneity of the adsorption was governed by the overall negative value of $\Delta G°$. The kinetic study showed that the adsorption of all the three phenols on zirconium-ferrite nanoparticles showed pseudo-second-order kinetic models.

Keywords: Zirconium-ferrite nanoparticles; Adsorption isotherm; Phenols; Langmuir isotherm

1. Introduction

The presence of phenol and its derivatives in drinking water, municipal water, and industrial wastewater has been a worldwide problem due to their high toxicity and carcinogenicity even at low concentrations. The presence of phenolic compounds in water may result in damage to various systems of the human body and also affects our environment. Phenol and its derivatives are widely used as intermediates in the synthesis of plastics, dyes, pesticides and insecticides [1–7]. Chlorophenol comes from various sources such as pesticide, paint, solvent, pharmaceutics, paper, pulp industries and water disinfecting processes [8]. Chlorophenols create complicated problems to water bodies such as bad odor and taste in drinking water, the death of aquatic life and inhibition of normal activities of

* Corresponding author.

the microbial population in wastewater treatment plants [9–13]. Nitrophenols also belong to a category of one of the most persistent and hazardous organic pollutants of industrial wastewater and exhibit high toxicity or mutagenicity directly or through its catabolic metabolites for living organisms [14–16]. Therefore, it is an issue of enormous interest to remove the phenols and its derivatives from contaminated water. Several methods have been used for the removal of phenol and its derivatives from wastewater. The important methods are coagulation, conventional oxidation methods by oxidizing agents, irradiation and electrochemical processes, membrane filtration, nanofiltration, reverse osmosis, electrodialysis and adsorption [17–27]. Most of the methods used for the removal of phenolic derivatives are associated with the involvement of hazardous organic solvents, expensive reagent, toxic by-product, drastic reaction condition, time-consuming and expensive. However, the adsorption technique has been found as one of the most prevalent techniques for the removal of pollutants from contaminated water. The common adsorbents used for the removal of pollutants are activated carbon, molecular sieves, polymeric adsorbents and some other low-cost materials [4,28,29]. Salam et al. [10] reported the removal of chlorophenol from aqueous solutions using multiwalled carbon nanotubes and their kinetic and thermodynamic studies. Abburi [11] studied the adsorption of both phenol and p-chlorophenol on Amberlite XAD-16 resin from their single and bisolute aqueous solutions. Ghaffari et al. [12] studied the adsorption of chlorophenols on amino-modified ordered nanoporous silica materials from aqueous solution. Li et al. [1] reported the surfactant-modified montmorillonite for the adsorption of phenol and also studied their mechanism, thermodynamics and regeneration process. Alshehri et al. [30] reported the adsorption of phenol using curcumin-based antimicrobial bio-adsorbent. The adsorption of phenolic compounds using various adsorbents, such as polypropylene powder (Accurel), powdered activated mustard cake, activated carbon and agro-waste [31–35]. Kumar et al. [36] reported the removal of bisphenol-A using ZnSe-WO_3 based nanomaterial. Dhiman et al. [37] studied solar powered degradation of bisphenol A from the aqueous environment using nano $Fe_xZn_{1-x}O$ as a tunable and efficient photocatalyst. Biochar-templated g-C_3N_4/$Bi_2O_2CO_3$/$CoFe_2O_4$ nano-assembly has also been employed for the photodegradation of nitrophenol [38]. Gold nanoparticles decorated multiwalled carbon nanotubes have also been used for the reduction of 4-nitrophenol [39].

Besides the above, numerous mixed metal oxides have been used as potential adsorbent for the removal of phenolic compounds [40–43]. The mixed metal oxide nanoparticle shows higher surface area, better adsorption capacities, more active sites than bulk materials, high efficiency and selectivity [44–46]. Among the various mixed metal oxides, zirconium-ferrite nanoparticles have extensively studied for the adsorption of heavy metal ions. Gupta et al. [47] have reported the synthesis and characterization of nanostructure iron(III)-zirconium(IV) binary mixed oxide and their use as an adsorbent for the adsorption of arsenic(III) from aqueous solution. The sorption of arsenic(V) on agglomerated nanostructure iron(III)-zirconium(IV) mixed oxide has also been studied [48]. Adsorptive removal of arsenic from water by an iron-zirconium oxide has also been studies by Ren et al. [49]. In their study, it has been reported that the adsorbent was amorphous and the specific surface area of the adsorbent was 339 m^2/g. Long et al. [50] reported the removal of phosphate from aqueous solution using magnetic iron-zirconium oxide with a specific surface area of 106.2 m^2/g. However, up to date literature survey reveals that no attempt, so far, has been made to utilize the adsorption potential of zirconium-ferrite nanoparticles for phenol, 2-chlorophenol and 2-nitrophenol. Therefore, we are interested to explore the adsorption efficiency of zirconium-ferrite nanoparticles for phenol, 2-chlorophenol and 2-nitrophenol. The results of adsorption of phenol, 2-chlorophenol and 2-nitrophenol on zirconium-ferrite nanoparticles and values of the thermodynamic parameter, namely, $\Delta G°$, $\Delta H°$ and $\Delta S°$ and the kinetic studies are being reported in the present contribution.

2. Experimental

2.1. Materials

Zirconium oxychloride octahydrate (Merck, New Delhi-110028), ferric chloride hexahydrate (Merck, New Delhi-110028), hydrochloric acid (Merck, New Delhi-110028), sodium hydroxide (Merck, New Delhi-110028), ethanol (Merck, New Delhi-110028), nitric acid (Merck, New Delhi-110028), phenol (Merck, New Delhi-110028), 2-chlorophenol (Merck, New Delhi-110028) and 2-nitrophenol (Merck, New Delhi-110028) were used as received. All other chemicals used were of analytical reagent grade. Deionized water was used throughout the experiment.

2.2. Synthesis of zirconium-ferrite nanoparticles

Zirconium-ferrite nanoparticles were synthesized by the co-precipitation technique [44]. In this method, 2.72 g of ferric chloride hexahydrate and 1.62 g of zirconium oxychloride octahydrate were dissolved, separately, in 50 mL deionized water. The solution of zirconium oxychloride was mixed dropwise in ferric chloride solution and stirred for 30 min at 65°C. To the above reaction mixture, a 3.5 M NaOH solution was drop-wise added with constant stirring, till its pH reaches up to 10. It resulted in the precipitation of chloride precursors in about 120 min. The above mixture was stirred for another 60 min. The precipitate was filtered and washed with doubly distilled water until it became free of chloride ions. The precipitate, so obtained, was dried at 100°C for 90 min in an oven. The solid material was crushed and then sieved with 100 μm mesh size.

2.3. Instrumentations

The characterization of the synthesized zirconium-ferrite nanoparticles was done using different analytical techniques. The X-ray diffraction (XRD) pattern was recorded on a Bruker D8 advance diffractometer (Billerica, Massachusetts, USA). The chemical composition was determined on the bases of energy dispersive X-ray (EDX) analysis. The scanning electron microscopy (SEM) measurement was recorded using a ZEISS (SUPRA) instrument. The transmission electron microscopy (TEM) of zirconium-ferrite nanoparticles was done using an FEI Tecnai T20 transmission electron microscope with a 200 keV electron source (FEI, Hillsboro, Oregon, United States). The thermal stability of zirconium-ferrite nanoparticles was analyzed by thermo-gravimetric

analyser (TGA 4000), PerkinElmer (Waltham, Massachusetts, U.S.A.), under a nitrogen atmosphere at a heating rate of 10°C/min from 30°C to 600°C. The zirconium-ferrite nanoparticles were also studied by Raman spectral studies using a Raman spectrometer (Research India, RIRMLP1519). A Zeta potential analyzer (Zetasizer ver.7.03 instrument, Malvern, MAL1093032, Malvern, Worcestershire, U.K.) was used to find out the isoelectric point of zirconium-ferrite nanoparticles. The Fourier transformed infrared (FT-IR) spectra of adsorbent and adsorbate–adsorbent adducts were recorded on a PerkinElmer (Waltham, Massachusetts, U.S.A.) 1600 FT-IR spectrophotometer using KBr pellets. The Brunauer–Emmett–Teller method was used to determine the surface area of the synthesized zirconium-ferrite nanoparticles.

2.4. Adsorption studies

The adsorption of phenol, 2-chlorophenol and 2-nitrophenol on the synthesized material was determined by batch adsorption technique. The adsorption of all three adsorbates was studied using their wide concentration range (20–100 mg/L). The pH of the adsorbate–adsorbent mixture was maintained by adding a tiny amount of concentrated hydrochloric acid or sodium hydroxide solution. The adsorption was carried out on adding a fixed amount of adsorbent on the 50 mL of adsorbate solution. The adsorbate–adsorbent mixture was vigorously agitated followed by filtration. The sample was taken from the adsorbate–adsorbent mixture at certain intervals of time. These samples were centrifuged, filtered and the filtrate was subjected to UV–Vis spectrophotometric analysis. The concentration of phenol, 2-chlorophenol and 2-nitrophenol before and after adsorption was analyzed by UV–Vis spectrophotometer at wavelength 270, 273 and 352 nm, respectively. In the preliminary stage, the effect of the reaction condition was studied by changing one reaction condition keeping all other conditions fixed. The adsorption (%) and adsorption capacity X_e (mg/g) was calculated by using the following equations:

$$\text{Adsorption}\% = \frac{C_0 - C_{eq}}{C_0} \times 100 \quad (1)$$

$$X_e = \frac{C_0 - C_{eq}}{m} \times V \quad (2)$$

where C_0 (mg/L) and C_{eq} (mg/L) are the concentration of the adsorbates in solution at initial and at equilibrium, respectively, V (L) is the total volume of adsorbates solution and m (g) is the mass of adsorbent.

3. Results and discussion

3.1. Characterization of zirconium-ferrite nanoparticles

The XRD pattern of the synthesized material is shown in Fig. 1 which showed two broad peaks at approximately 32.5° and 63.2° which resembled previously reported two-line ferrihydrite [51,52]. This observation indicates the synthesized material is amorphous and similar to two-line ferrihydrite [49,53].

The specific surface area of the synthesized zirconium-ferrite nanoparticles was found to be 392 m^2/g with a pore volume of 0.1723 cm^3/g and mean pore diameter is 6.0792 nm in the present contribution. Ren et al. [49] reported the surface area of Fe-Zr binary oxide was found to be the surface area of 339 m^2/g with a pore volume of 0.21 cm^3/g. Thus, the zirconium-ferrite nanoparticles, synthesized in the present study, showed a higher surface area than that of the previously reported zirconium-ferrite nanoparticles.

The SEM–EDX of the synthesized zirconium-ferrite nanoparticles has been shown in Fig. 2, which showed their rough surfaces and porous structure [49]. The EDX showed the atomic percentage of Zr/Fe is 15.23/10.53 in the synthesized material.

Further, the synthesized zirconium-ferrite nanoparticles were examined by TEM and the TEM image has been shown in Fig. 3, which showed that the particle size range is of 16–20 nm. The TEM analysis of the zirconium-ferrite nanoparticles was found to be 34 nm in previously reported work [45]. Therefore, the zirconium-ferrite nanoparticles, synthesized in the present study, were consisting of smaller particle size than that of the reported one.

The zeta potential of zirconium-ferrite nanoparticles was determined over a wide range of pH (2.0 to 9.0) and the results have been shown in Fig. 4. The isoelectric point of zirconium-ferrite nanoparticles was found to be 3.92. It reveals that at pH 3.92, zirconium-ferrite nanoparticles have a positively charged surface and can act as an anion exchanger. On the other hand, at pH greater than 3.92, the surface of zirconium-ferrite nanoparticles gets negatively charged, which favors more adsorption of cations [54].

The thermo-gravimetric analysis (TGA) of zirconium-ferrite nanoparticles has been carried out and the TGA curve has been shown in Fig. 5. The synthesized zirconium-ferrite nanoparticles showed nearly 12% weight loss at 100°C and 25% weight loss in the range of 200°C–600°C. The weight loss of up to 100°C may be due to the evaporation of water contents [55].

The functionalization of zirconium-ferrite nanoparticles was also confirmed by Raman spectral studies and the Raman spectrum has been shown in Fig. 6. The Raman spectrum of zirconium-ferrite nanoparticles showed the characteristics bands at 197, 393, 452, 613, 705 and 840 cm^{-1}. The bands at 197, 393, 452 and 613 cm^{-1} may be assigned for the Zr ion in the synthesized material [56]. The bands appeared at 705 and 840 cm^{-1} may be due to the presence of Fe ion in the synthesized materials. Li et al. [57] has been reported the same observation for the Raman spectrum ofiron oxide nanoparticles.

The functional groups present in the synthesized material were determined using FT-IR spectral studies and the FT-IR spectrum has been shown in Figs. 7a–d. It shows the bands at 442; 540; 1,346; 1,570 and 3,414 cm^{-1}. Broadband at 3,414 cm^{-1} should be assigned for O–H stretching vibration of water molecules and the bands at 1,570 and 1,346 cm^{-1} may be corresponding to O–H bending vibrations [55,58]. The bands at 540 and 442 cm^{-1} may be assigned for the metal-oxygen stretching vibration in the synthesized material [59]. The FT-IR spectra of zirconium-ferrite nanoparticles before and after adsorption of phenol, 2-chlorophenol and 2-nitrophenol have been shown in Figs. 7a–d. It is observed from the FT-IR spectra that no new peak has appeared after adsorption of

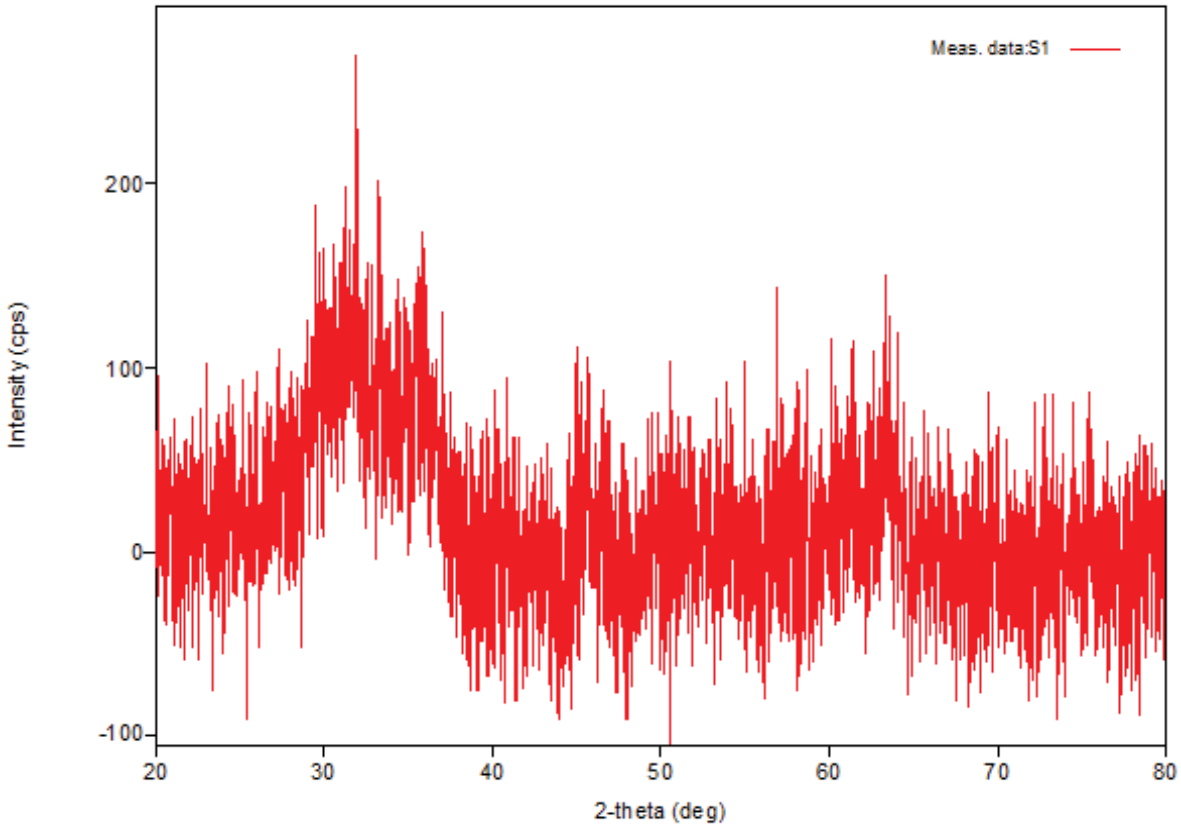

Fig. 1. XRD pattern of zirconium-ferrite nanoparticles.

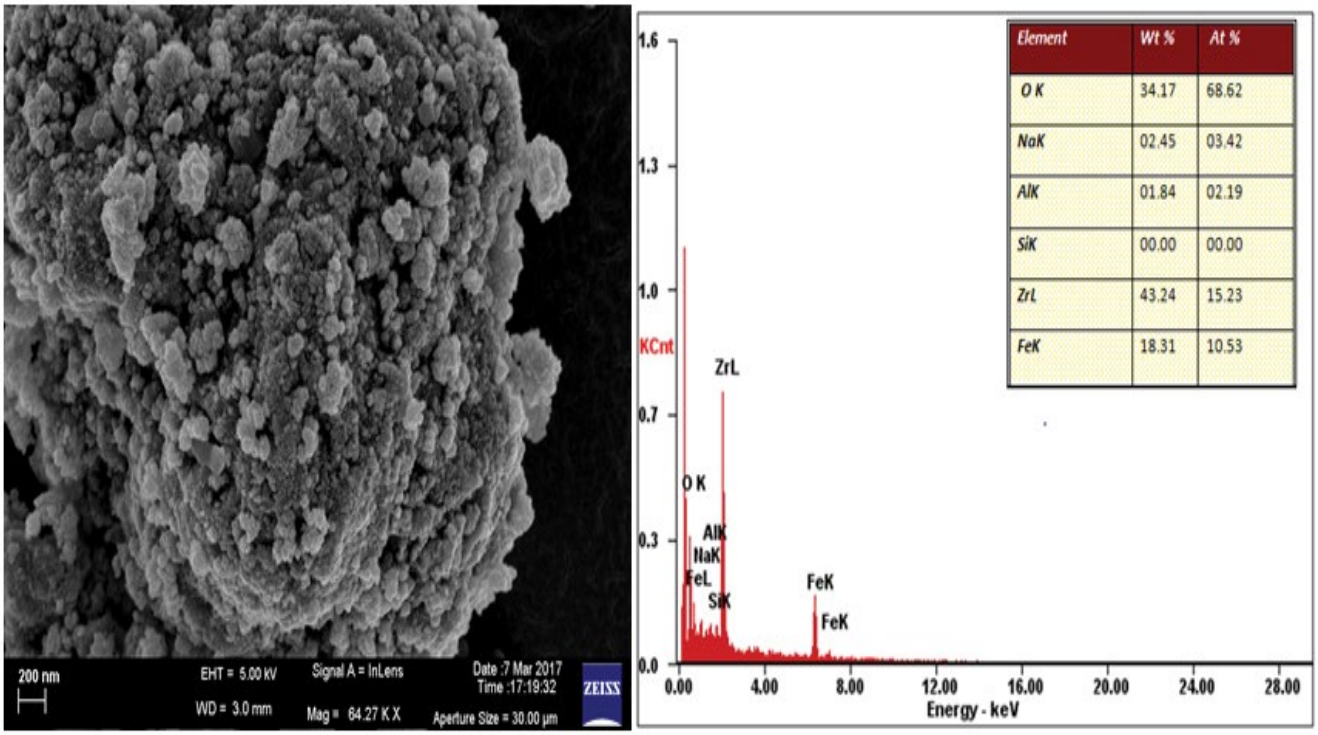

Fig. 2. SEM–EDX image of zirconium-ferrite nanoparticles.

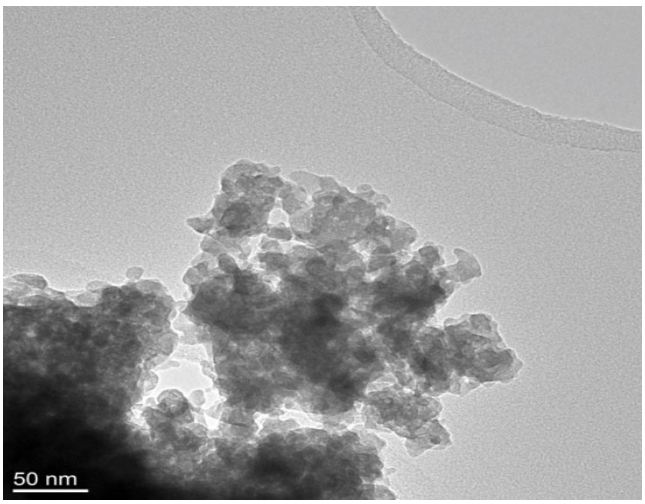

Fig. 3. TEM image of zirconium-ferrite nanoparticles.

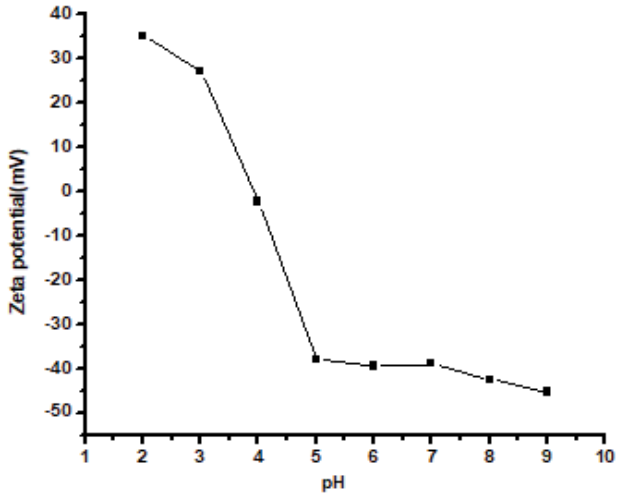

Fig. 4. Zeta potential graph of zirconium-ferrite nanoparticles.

phenol, 2-chlorophenol and 2-nitrophenol on zirconium-ferrite nanoparticles. Further, a significant shift in the peaks was not found in the FT-IR spectrum of zirconium-ferrite nanoparticles after adsorption of phenol, 2-chlorophenol and 2-nitrophenol. These results reveal that the adsorption of phenol, 2-chlorophenol and 2-nitrophenol on zirconium-ferrite nanoparticles took place through the involvement of weak Van der Waals interaction without any interaction chemical in nature. The adsorption of phenols on zirconium-ferrite nanoparticles seems to be due to hydrogen bond. This fact is evident from broadband in phenol, 2-chlorophenol and 2-nitrophenol.

3.2. Effect of process parameters on phenol, 2-chlorophenol and 2-nitrophenol adsorption

3.2.1. Effect of the amount of zirconium-ferrite nanoparticles

The effect of the amount of zirconium-ferrite nanoparticles on the adsorption of phenol, 2-chlorophenol and

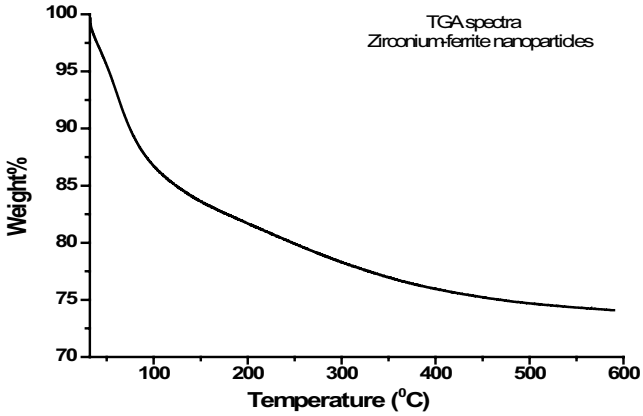

Fig. 5. TGA graph of zirconium-ferrite nanoparticles.

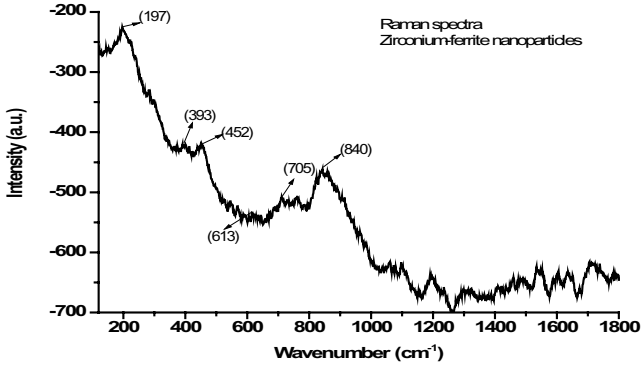

Fig. 6. Raman spectra of zirconium-ferrite nanoparticles.

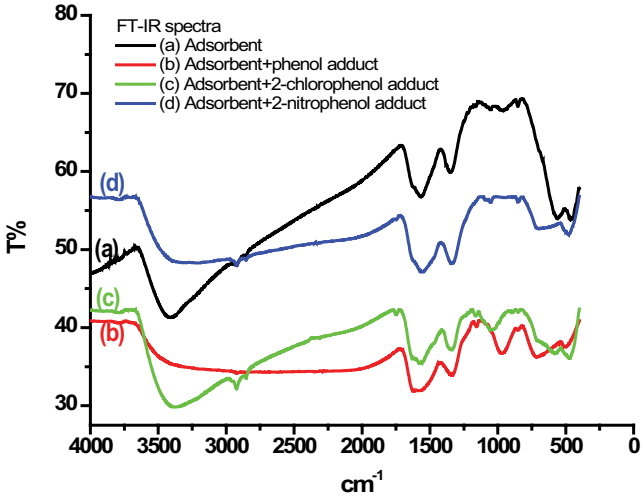

Fig. 7. Fourier transform infrared (FT-IR) spectra of (a) zirconium-ferrite nanoparticles, (b) zirconium-ferrite nanoparticles-phenol adduct, (c) zirconium-ferrite nanoparticles-2-chlorophenol adduct, (d) zirconium- ferrite nanoparticles-2-nitrophenol adduct.

2-nitrophenol has been evaluated at a different adsorbent dose at the fixed phenolic concentration (20 mg/L and pH 4.0). The dose of adsorbent from 0.05 to 0.5 g/L solution has been used in this study to determine the optimum

adsorbent dose and the results have been shown in Fig. 8a. It showed that the percentage adsorption of phenols was also increased by increasing the amount of zirconium-ferrite nanoparticles from 0.05 to 0.3 g. This increase can be attributed because more adsorption sites will be available for adsorption on the increasing amount of adsorbent from 0.05 to 0.3 g [60]. However, the percentage adsorption of phenols exhibited no further appreciable increase in increasing the amount of adsorbent above 0.3–0.5 g. Hence, an optimum amount of 0.3 g zirconium-ferrite nanoparticles was used for the subsequent adsorption studies.

3.2.2. Effect of pH

The effect of the pH change on the adsorption of phenols on zirconium-ferrite nanoparticles was studied by varying the solution pH from 2 to 12, while all the other parameters including contact time, adsorbent dosage, initial concentration and temperature were kept constant at 120 min, 0.3 g, 20 mg/L and 288 K, respectively. The effect of pH on the adsorption of phenols has been shown in Fig. 8b. The zeta potential value (pH_{zpc}) of the zirconium-ferrite nanoparticles was found to be 3.92 (Fig. 4). When the pH is below 3.92, the zirconium-ferrite nanoparticles remain positively charged and above this pH value, the surface of the zirconium-ferrite nanoparticles acquires a negative charge. The pKa value of phenol, 2-chlorophenol and 2-nitrophenol are 10, 8.5 and 7.2, respectively. If the pH of the solution is below pKa value then the phenols will be in the protonated state and above this value, it exists as negatively charged phenolate ions. The turning point of adsorption efficiency of phenol, 2-chlorophenol and 2-nitrophenol on zirconium-ferrite nanoparticles were found at pH nearly 8.0, 6.0 and 4.0, respectively. This change could be attributed to the zeta potential value (pH_{zpc}) of the adsorbent. Thus, below pH 4.0, the ionization is possible only for 2-nitrophenol due to the presence of an ionized negatively charged nitro-group and which shows electrostatic attraction with the positively charged adsorbent. Above pH 4.0, the adsorption of 2-nitrophenol was decreased. However, in the case of phenol and 2-chlorophenol, the pH hardly affects the adsorption efficiency in the pH range of 4.0 to 6 as shown in Fig. 8b. Therefore, the maximum adsorption of phenol, 2-chlorophenol and 2-nitrophenol was found to be at pH 4.0 and it was selected as optimized pH value for subsequent adsorption study. On the basis of pH studies, a possible mechanism of adsorption of phenols on zirconium-ferrite nanoparticles can be presented under the following steps:

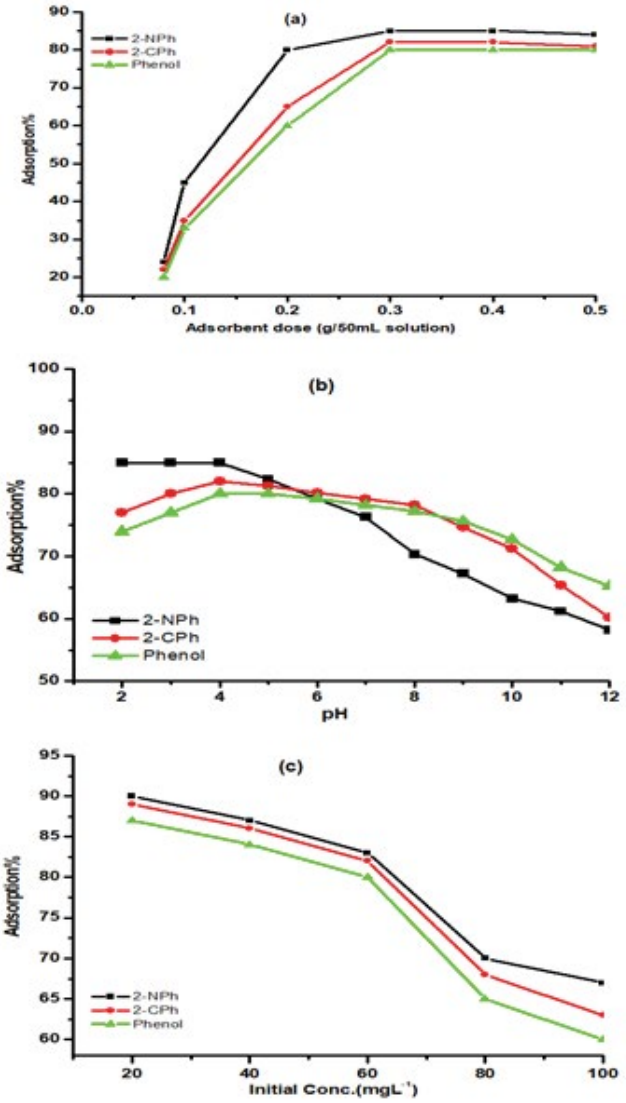

Fig. 8. Effect of (a) adsorbent dose, (b) pH and (c) initial concentration of adsorbate on percentage adsorption of phenol, 2-chlorophenol and 2-nitrophenol.

- *Step (i)*: At pH above to 8, 5.5 and 4 for phenol, 2-chlorophenol and 2-nitrophenol, respectively, get ionized as under:

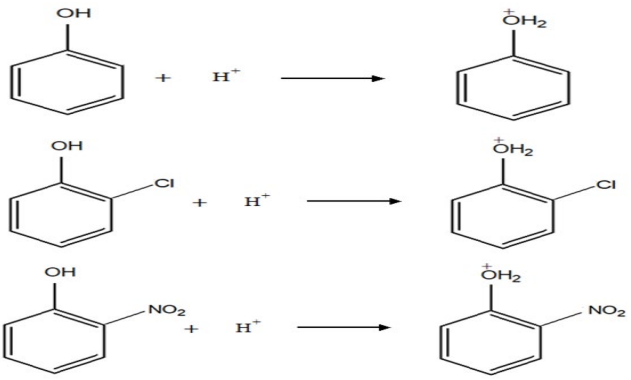

- *Step (ii)*: Above to pH 3.92 the surface of zirconium-ferrite nanoparticles acquires a negative charge.

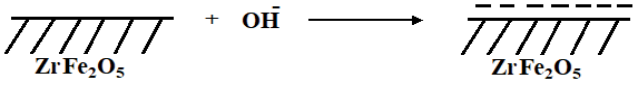

- *Step (iii)*: Adsorption proceeds through interaction between the positively charged surface of phenols and negatively charged surface of zirconium-ferrite nanoparticles.

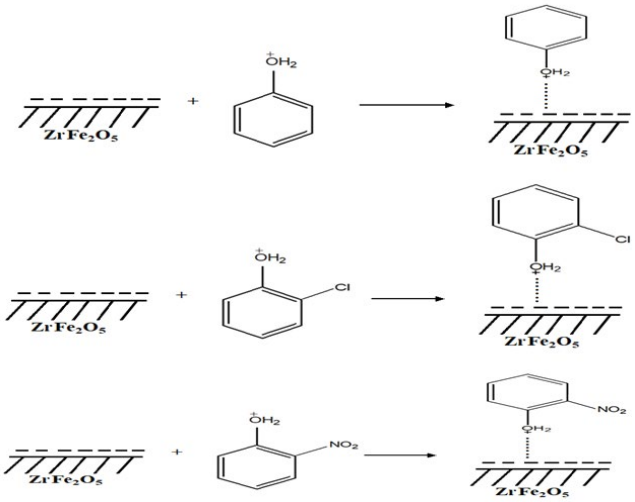

3.2.3. Effect of adsorbates concentration

The initial concentration of the adsorbates was varied from 20 to 100 mg/L of phenol, 2-chlorophenol and 2-nitrophenol for the evaluation of percentage adsorption. Adsorption conditions, such as pH, contact time, adsorbent dose and temperature were kept constant at 4.0, 120 min, 0.3 g/L solution and 288 K, respectively. The percentage adsorption of all the phenolic compounds at various initial concentrations for a fixed amount of adsorbent (0.3 g/L of solution) and pH (4.0) is shown in Fig. 8c. It was observed that the percentage adsorption was decreased when the adsorbate concentration was gradually increased which may be due to saturation of available adsorption sites on the surface of zirconium-ferrite nanoparticles. Hence, in the present study, the optimum concentration of the phenolic compounds is found to be 20 mg/L.

3.2.4. Effect of contact time

The effect of time for the adsorption of phenol, 2-chlorophenol and 2-nitrophenol on zirconium-ferrite nanoparticles was performed by varying the contact time from 20 to 120 min. All the other parameters namely, adsorbent dosage (0.3 g/L solution), initial concentration (20 mg/L), pH (4.0) and temperature (288 K) were kept constant. The results have been shown in Fig. 9a, which showed that the adsorption of phenol increases on increasing the contact time from 20 to 120 min. No significant increase in the present adsorption was reported on a further increase in contact time from 120 to 160 min. Therefore, 120 min was found at the optimum time. It may be because the binding sites of adsorbent became exhausted and the uptake rate slowed due to competition for decreasing the availability of active sites by phenols.

3.2.5. Effect of temperature

The effect of temperature on adsorption of phenol, 2-chlorophenol and 2-nitrophenol on zirconium-ferrite nanoparticles has been studied by varying the temperature from

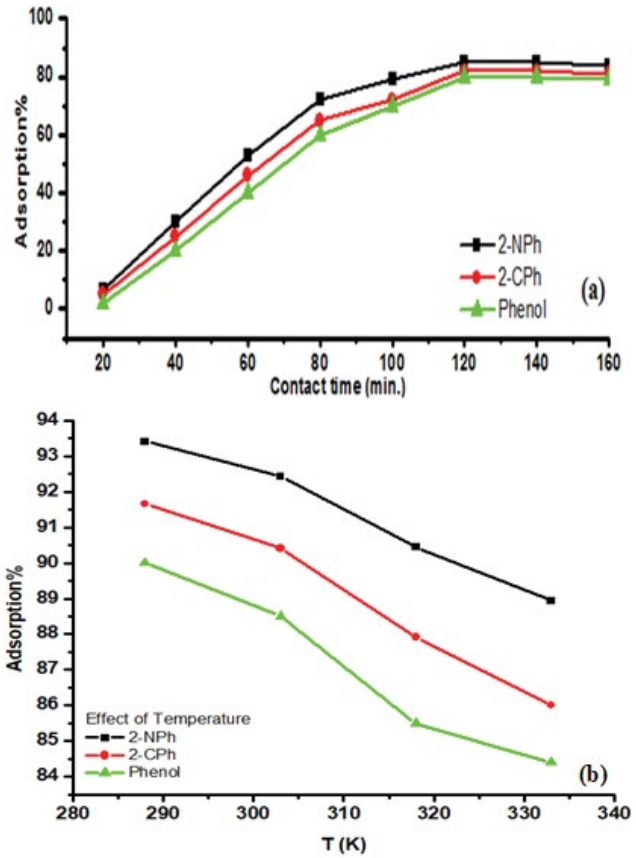

Fig. 9. Effect of (a) contact time, (b) temperature for the adsorption of phenol, 2-chlorophenol and 2-nitrophenol on zirconium-ferrite nanoparticles.

288 to 333 K and results have been shown in Fig. 9b. All the other parameters were kept constant such as adsorbent dosage (0.3 g/L solution), initial concentration (20 mg/L), pH (4.0) and contact time (120 min). The results clearly showed that the degree of adsorption goes to decrease on increasing the temperature from 288 to 333 K. It may be attributed to the exothermic nature of adsorption of all three phenols studied herein. Zhang et al. [61] reported that the removal efficiency of p-nitrophenol on nanographite oxide decreased on increasing the temperature, and indicate that the adsorption reactions are exothermic. Li et al. [63] reported that the adsorption of phenol, p-chlorophenol and p-nitrophenol on chitosan decreased on increasing temperatures.

3.3. Isotherm studies

The relationship between the amount of adsorbate adsorbed and its concentration in equilibrium solution at a constant temperature was described by adsorption isotherm studies. In the present study, several isotherms model, such as Langmuir, Freundlich and Temkin were applied to examine the adsorption of phenol, 2-chlorophenol and 2-nitrophenol on zirconium-ferrite nanoparticles. All graphs, of isothermal studies, have been shown in Supplementary data (Figs. S2–S4).

Langmuir adsorption isotherm exhibits the adsorption involved in the formation of a monolayer of phenol, 2-chlorophenol and 2-nitrophenol on the surface of zirconium-ferrite nanoparticles. The equation of Langmuir isotherm is given as under:

$$\frac{C_{eq}}{X_e} = \frac{1}{K_L X_m} + \frac{C_{eq}}{X_m} \tag{3a}$$

or

$$\frac{1}{X_e} = \frac{1}{C_{eq}} \frac{1}{K_L X_m} + \frac{1}{X_m} \tag{3b}$$

where C_{eq} is the concentration of adsorbate at equilibrium stage (mg L^{-1}), X_e is the amount of adsorbate adsorbed at equilibrium. X_m is the amount of adsorbate required for the complete monolayer formation over the surface of 1 g zirconium-ferrite nanoparticles, K_L is the Langmuir equilibrium constant which is related to the affinity of binding sites and energy of adsorption. The plot of $1/X_e$ vs. $1/C_{eq}$ showed a straight line and the value of K_L and X_m were determined from the slope and intercept, respectively.

The Freundlich isotherm is employed by assuming a heterogeneous surface with a non-uniform distribution of heat of adsorption over the surface. The equation of Freundlich isotherm is as follows:

$$X_e = K_F C_e^{1/n} \tag{4a}$$

This equation can be linearized as under:

$$\ln X_e = \ln K_F + \frac{1}{n} \ln C_e \tag{4b}$$

where X_e (mg/g) is the amount of phenols adsorbed per unit weight of zirconium-ferrite nanoparticles, C_e (mg/L) is the equilibrium concentration of solute, K_F (mg/g) and $1/n$ are Freundlich constants corresponding to adsorption capacity and adsorption intensity, respectively [59].

Temkin isotherm is based on the assumption that the heat of adsorption would decrease linearly with the increase of coverage of adsorbent and equation is given as follows:

$$X_e = \frac{RT}{b} \ln\left(K_T C_e\right) \tag{5a}$$

The linearized form of this equation is as follows:

$$X_e = B_1 \ln K_T + B_1 \ln C_e \tag{5b}$$

where $B_1 = RT/b$ and b (J mol^{-1}) is the Temkin energy constant. The factor K_T in this isotherm explicitly takes into account the interactions between adsorbing species and the adsorbent. A plot of X_e vs. ln C_e enables the determination of the isotherm constants b, B_1 and K_T from the slope and intercept, respectively, and values have been mentioned in Table 1 [59].

The results of isothermal studies for the adsorption of phenol, 2-chlorophenol and 2-nitrophenol on zirconium-ferrite nanoparticles showed that the adsorption data were found to follow Langmuir adsorption isotherm satisfactorily than Freundlich and Temkin adsorption isotherm. In Langmuir adsorption isotherm, all linear coefficients, R^2 were found to be greater than 0.990 (Table 1). In the present study, the adsorption capacity of zirconium-ferrite nanoparticles was found to be 334.44, 354.61 and 375.93 mg/g for phenol, 2-chlorophenol and 2-nitrophenol, respectively. The adsorption capacity of zirconium-ferrite nanoparticles was found to be maximum in comparison with the other adsorbents as mentioned in Table 2.

3.4. Thermodynamic analysis

A thermodynamic study of adsorption of phenol, 2-chlorophenol and 2-nitrophenol on the synthesized zirconium-ferrite nanoparticles has been carried out. The Gibbs free energy change ($\Delta H°$) values can confirm whether a process is spontaneous or non-spontaneous. The change in enthalpy ($\Delta H°$) provides information about the nature of adsorption either it is exothermic or endothermic and also differentiate between physical and chemical adsorption processes. The entropy change ($\Delta S°$) predicts the magnitude of changes in the adsorbent surface [33–35]. The change in Gibbs free energy ($\Delta G°$) was determined using the following equation:

$$\Delta G° = -RT \ln K_c \tag{6}$$

where R, T and K_c stand for is the universal gas constant, temperature (K) and equilibrium constant, respectively. The values of equilibrium constant were calculated using the following equation [59]:

$$K_c = \frac{C_{Ae}}{C_e} \tag{7}$$

Table 1
Adsorption isotherm parameters for the adsorption of phenol, 2-chlorophenol and 2-nitrophenol on zirconium ferrite nanoparticles at 288 K temperature

Adsorbate	Langmuir isotherm			Freundlich isotherm			Temkin isotherm		
	X_m (mg/g)	K_L (L/mg)	R^2	K_F (mg/g)	n	R^2	B_1(mg/g)	K_T	R^2
Phenol	334.44	0.108	0.994	41.44	1.67	0.979	29.85	0.94	0.932
2-Chlorophenol	354.61	0.124	0.995	46.67	1.64	0.982	28.31	1.09	0.934
2-Nitrophenol	375.93	0.150	0.995	54.61	1.61	0.984	26.85	1.33	0.936

Table 2
Adsorption capacity comparison of zirconium-ferrite nanoparticles for phenol, 2-chlorophenol and 2-nitrophenol with that of different adsorbents

Adsorbent	Adsorption capacity (mg/g)			Reference
	Phenol	2-Chlorophenol	2-Nitrophenol	
ANL	69.70	–	–	[70]
Sewage sludge	94.00	–	–	[71]
Activated sludge	86.10	–	–	[72]
Activated sewage sludge	29.46	–	–	[73]
Pyrolysed sewage sludge	5.56	–	–	[73]
Lignite	10.00	–	–	[74]
Fly ash	–	98.70	–	[75]
Aged-refuse in biofilter	–	1.27	–	[76]
Sargassum muticum	–	79.00	–	[77]
Red mud	–	117.30	–	[78]
Chitosan	–	70.52	–	[79]
FA	–	–	6.44	[80]
Wood FA	–	–	143.80	[81]
Zirconium-ferrite nanoparticles	334.44	354.61	375.93	Present study

where C_{Ae} and C_e are the equilibrium concentrations (mg/L) of phenols on the adsorbent and in solution, respectively.

The values of $\Delta H°$ and $\Delta S°$ have been determined using Van't Hoff model:

$$\ln K_c = \frac{\Delta S°}{R} - \frac{\Delta H°}{RT} \quad (8)$$

At different temperatures, the different values of $\ln K_c$ were obtained and the graphs between $\ln K_c$ vs. $1/T$ were plotted (Fig. S1) and the values of slope and intercept were used to determine $\Delta H°$ and $\Delta S°$, respectively, from Van't' Hoff plot [64]. The results of the thermodynamic studies have been shown in Table 3.

The values of $\Delta G°$ at all temperatures (288–333 K) were found to be negative in the range of –4.60 to –6.33 for all the three phenols. It shows that the adsorption process involved physical forces between adsorbate and adsorbent and it occurs spontaneously [65]. The $\Delta G°$ value has been reported to be −20 to 0 kJ/mol for physical adsorption and the $\Delta G°$ value for chemisorption varies between −80 and −400 kJ/mol [66–68]. Silva et al. [69] reported the thermodynamic study of adsorption of phenol, 4-chlorophenol and 4-nitrophenol on activated carbon and the free energy was observed from −0.63 to −5.76 kJ/mol. Zhang et al. [61] investigated the adsorption of p-nitrophenol from aqueous solutions using nanographite oxide.

The $\Delta H°$ values are negative for all of the phenols, showing the exothermic nature of the adsorption process and the values were found to be –9.55, –10.64 and –9.74 kJ mol^{-1} for phenol, 2-chlorophenol and 2-nitrophenol, respectively. These enthalpies represent the energy released on the adsorbate–adsorbent interface during the interaction of all three phenols on zirconium-ferrite nanoparticles. The value of $\Delta H°$ as observed in the present study showed that the adsorption of all three phenols involves the weak interaction with zirconium-ferrite nanoparticles which showed physisorption [66,68]. Zhang et al. [61] have also reported the negative value of $\Delta H°$ for the adsorption of p-nitrophenol onto nanographite oxide. They found the value of $\Delta H°$ was –17.43 J/mol K and confirmed the adsorption process was exothermic and physical in nature [61]. Silva et al. [69] also found the negative values of $\Delta H°$ for the adsorption of phenol, 4-nitrophenol and 4-chlorophenol and proved that the adsorption of all these phenols is exothermic process.

The values of $\Delta S°$ were found to be –0.014, –0.016 and –0.011 J/mol K for phenol, 2-chlorophenol and 2-nitrophenol, respectively. The decrease in $\Delta S°$ value revealed the lowering

Table 3
Thermodynamic parameters for the adsorption of phenol, 2-chlorophenol and 2-nitrophenol on zirconium-ferrite nanoparticles

Adsorbate	T (K)	Thermodynamic parameters		
		$\Delta G°$ (kJ/mol)	$\Delta H°$ (kJ/mol)	$\Delta S°$ (J/mol K)
Phenol	288	–5.27	–9.55	–0.014
	303	–5.05		
	318	–4.83		
	333	–4.60		
2-CP	288	–5.79	–10.64	–0.016
	303	–5.54		
	318	–5.29		
	333	–5.03		
2-NP	288	–6.33	–9.74	–0.011
	303	–6.15		
	318	–5.98		
	333	–5.80		

in randomness at the solid–liquid interface and the internal structure of adsorbent did not get affected during adsorption [66]. The $\Delta S°$ value showed the non-spontaneous nature of the adsorption process. Zhang et al. [61] also examined the negative value of $\Delta S°$ for the adsorption of p-nitrophenol onto nanographite oxide. Overall, the spontaneity of the adsorption process was governed by the negative value of $\Delta G°$ [61].

3.5. Adsorption kinetics

The kinetic parameters for the adsorption of phenol, 2-chlorophenol and 2-nitrophenol on zirconium-ferrite nanoparticles at 288 K were studied. In this study, the experimental data were fitted in pseudo-first-order and pseudo-second-order equations to find out adsorption kinetics. The pseudo-first-order-kinetic model is given as:

$$\ln\left(q_e - q_t\right) = \ln q_e - k_1 t \tag{9}$$

where q_e (mg/g) is the amount of phenol, 2-chlorophenol and 2-nitrophenol adsorbed per unit weight of the zirconium-ferrite nanoparticles at equilibrium (mg/g), q_t (mg/g) is the amount of phenol, 2-chlorophenol and 2-nitrophenol adsorbed at any time. The t stands for time (min) and k_1 is pseudo-first-order rate constant of adsorption (1/min). The values of slope and intercept of the plot of ln (q_e–q_t) vs. t, were used to determine k_1 and q_e, respectively, and values have been mentioned in Table 4 and Fig. S5.

The pseudo-second-order kinetic model for the adsorption of phenol, 2-chlorophenol and 2-nitrophenol on zirconium-ferrite nanoparticles is expressed as:

$$\frac{t}{q_t} = \frac{1}{k_2 q_e^2} + \frac{1}{q_e} t \tag{10}$$

where q_e (mg/g) is the amount of phenol, 2-chlorophenol and 2-nitrophenol adsorbed per unit weight of the zirconium-ferrite nanoparticles at equilibrium (mg/g). q_t (mg/g) is the amount of phenol, 2-chlorophenol and 2-nitrophenol adsorbed at any time. The t stands for time (min) and k_2 stands for the equilibrium constant in the pseudo-second-order reaction. In the pseudo-second-order kinetic model, the plot of t/q_t vs. t was used to determine the value of q_e and k_2 from the slope and intercept, respectively (Fig. S6) and values have been mentioned in Table 4.

From the values of Table 4, it is clear that the calculated value of q_e in pseudo-first-order kinetic was not in good agreement with the experimental value of q_e. The results indicate that the adsorption of all three phenols on zirconium-ferrite nanoparticles does not follow pseudo-first-order kinetics. From Table 4, it is clear that the calculated values of q_e are in good agreement with the experimental value of q_e and the correlation coefficient (R^2) for pseudo-second-order kinetics is greater than 0.999. It confirmed that the adsorption of all three phenols on zirconium-ferrite nanoparticles follows pseudo-second-order kinetics.

3.6. Desorption of phenols using different solvents

In the desorption experiment, the used zirconium-ferrite nanoparticles after the adsorption of phenols were taken out from the solution and washed with distilled water and dried at 120°C in an oven for 4 h. The solvents, namely, sodium hydroxide, ethanol and hydrochloric acid have been used for desorption of phenols from zirconium-ferrite nanoparticles and results have been shown in Fig. 10. The zirconium-ferrite nanoparticles after the adsorption of phenols were put into 20 mL of NaOH solution and the mixture was then shaken in the thermostatic shaker at room temperature for

Table 4
Kinetic parameters of pseudo-first and pseudo-second-order for the adsorption of phenol, 2-chlorophenol and 2-nitrophenol on zirconium-ferrite nanoparticles

Adsorbate		Pseudo-first-order kinetics				Pseudo-second-order kinetics		
Initial concentration (mg/L)		$q_{e,\exp}$ (mg/g)	$q_{e1,\text{cal}}$ (mg/g)	k_1 (1/min)	R^2	$q_{e2,\text{cal}}$ (mg/g)	k_2 (g/mg min)	R^2
Phenol	20	1.07	2.92	1.43×10^{-2}	0.990	1.07	0.42×10^{8}	1.00
	40	4.02	11.98	3.04×10^{-2}	0.992	4.02	11.00×10^{8}	1.00
	60	8.97	26.40	4.81×10^{-2}	0.942	8.97	23.00×10^{8}	1.00
	80	16.02	9.06	1.93×10^{-2}	0.948	16.02	54.00×10^{8}	1.00
	100	18.59	14.51	2.59×10^{-2}	0.960	18.59	0.80×10^{8}	1.00
2-CP	20	1.01	3.37	2.35×10^{-2}	0.964	1.01	1.31×10^{8}	1.00
	40	3.02	8.33	2.27×10^{-2}	0.988	3.01	2.10×10^{8}	1.00
	60	6.02	10.44	2.55×10^{-2}	0.988	6.02	2.50×10^{8}	1.00
	80	13.92	12.90	3.25×10^{-2}	0.991	13.92	0.04×10^{8}	1.00
	100	15.03	11.57	2.33×10^{-2}	0.985	15.03	0.06×10^{8}	1.00
2-NP	20	1.31	1.03	0.58×10^{-2}	0.962	1.30	2.04×10^{8}	1.00
	40	2.86	10.40	4.0×10^{-2}	0.982	2.86	0.41×10^{8}	1.00
	60	5.39	8.80	2.5×10^{-2}	0.992	5.38	0.11×10^{8}	1.00
	80	10.02	9.10	2.1×10^{-2}	0.993	10.02	0.20×10^{8}	1.00
	100	11.13	17.30	2.7×10^{-2}	0.975	11.12	0.09×10^{8}	1.00

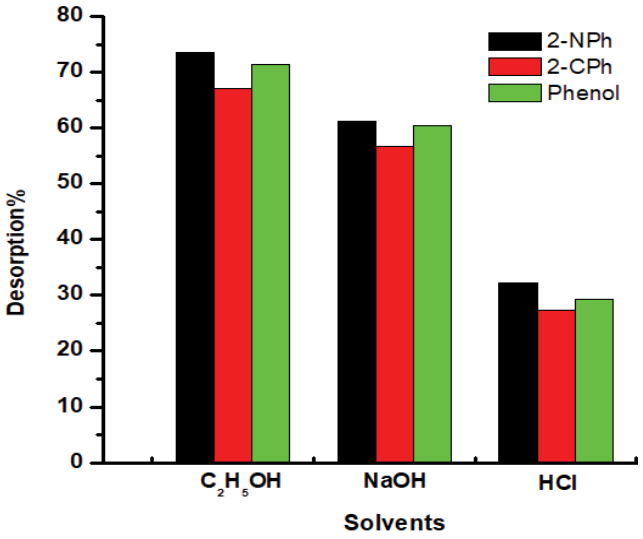

Fig. 10. Effect of different solvents on the percentage desorption of phenol, 2-chlorophenol and 2-nitrophenol

3 h. The same process was repeated for the remaining two solvents, ethanol and hydrochloric acid. After desorption, the mass of phenols desorbed was analyzed in the liquid phase using the UV–vis spectrophotometer. The desorption percentage was determined using the following expression.

$$\text{Desorption}\% = \frac{\text{Mass of phenols desorbed}}{\text{Mass of phenols adsorbed}} \times 100 \qquad (11)$$

The desorption percentage of phenol with ethanol, sodium hydroxide and hydrochloric acid solvents was found to be 71.34%, 60.46% and 29.34%, respectively. The desorption percentage of 2-chlorophenol was found to be 67.12%, 56.72% and 27.32% with ethanol, sodium hydroxide and hydrochloric acid solvents, respectively. For 2-nitrophenol, the desorption percentage was found to be 73.52%, 61.21% and 32.28% with ethanol, sodium hydroxide and hydrochloric acid, respectively. Hence, in the present study, ethanol was found to show the maximum desorption efficiency for phenols than sodium hydroxide and hydrochloric acid.

4. Conclusion

The present study showed a high adsorption potential of zirconium-ferrite nanoparticles for phenol, 2-chlorophenol and 2-nitrophenol. The synthesized zirconium-ferrite nanoparticles have been found as improved nanomaterial in terms of high surface area (392 m^2/g) with a pore volume of 0.1723 cm^3/g and the mean pore diameter of 6.0792 nm. The adsorption data were found to follow the Langmuir isotherm trend. Therefore, the adsorption capacities (at 288 K) on synthesized material for phenol, 2-chlorophenol and 2-nitrophenol were found to be 334.44, 354.61 and 375.93 mg/g, respectively. The results of the thermodynamic study showed that the adsorption was exothermic in nature and take place through a physisorption process spontaneously. The results of the kinetic study showed that the adsorption of all three phenols on zirconium-ferrite nanoparticles showed the pseudo-second-order kinetic model.

Acknowledgments

One of the authors is highly thankful to "University Grant Commission, New Delhi" for "Rajiv Gandhi National Fellowship (RGNF)" (Letter number F1-17.1/2016-17/RGNF-2015-17-SC-UTT-15953). Authors (AK, AGS and SRA) extend their appreciation to the Deanship of Scientific Research at King Khalid University for funding this work through Research groups program under grant number R.G.P. 2/36/40.

References

[1] Y. Li, X. Hu, X. Liu, Y. Zhang, Q. Zhao, P. Ning, S. Tian, Adsorption behavior of phenol by reversible surfactant-modified montmorillonite: mechanism thermodynamics and regeneration, Chem. Eng. J., 334 (2018) 1214–1221.
[2] H. Niu, Y. Zheng, S. Wang, L. Zhao, S. Yang, Y. Cai, Continuous generation of hydroxyl radicals for highly efficient elimination of chlorophenols and phenols catalyzed by heterogeneous Fenton-like catalysts yolk/shell Pd@Fe_3O_4@metal organic frameworks, J. Hazard. Mater., 346 (2018) 174–183.
[3] B. Shah, R. Tailor, A. Shah, Sorptive sequestration of 2-chlorophenol by zeolitic materials derived from bagasse fly ash, J. Chem. Technol. Biotechnol., 86 (2011) 1265–1275.
[4] R.L. Tseng, K.T. Wu, F.C. Wu, R.S. Juang, Kinetic studies on the adsorption of phenol, 4-chlorophenol and 2,4-dichlorophenol from water using activated carbons, J. Environ. Manage., 91 (2010) 2208–2214.
[5] X. Li, Y. Houa, Q. Zhaoa, W. Tenga, X. Hua, G. Chen, Capability of novel $ZnFe_2O_4$ nanotube arrays for visible-light induced degradation of 4-chlorophenol, J. Chemo., 82 (2011) 581–586.
[6] N. Roostaei, F.H. Tezel, Removal of phenol from aqueous solutions by adsorption, J. Environ. Manage., 70 (2004) 157–164.
[7] M.H. Entezari, C. Petrier, P. Devidal, Sonochemical degradation of phenol in water: a comparison of classical equipment with a new cylindrical reactor, Ultrason. Sonochem., 10 (2003) 103–108.
[8] O. Hamdaoui, E. Naffrechoux, Modeling of adsorption isotherms of phenol and chlorophenols onto granular activated carbon, part I: two-parameter models and equations allowing determination of thermodynamic parameters, J. Hazard. Mater., 147 (2007) 381–394.
[9] S. Xue, C. Wang, Y. Wei, Preparation of magnetic mesoporous carbon from polystyrene-grafted magnetic nanoparticles for rapid extraction of chlorophenols from water samples, RSC Adv., 7 (2017) 11921–11928.
[10] M.A. Salam, M. Mokhtar, S.N. Basahel, S.A. Al-Thabaiti, A.Y. Obaid, Removal of chlorophenol from aqueous solutions by multiwalled carbon nanotubes: kinetic and thermodynamic studies, J. Alloys Compd., 500 (2010) 87–92.
[11] K. Abburi, Adsorption of phenol and p-chlorophenol from their single and bisolute aqueous solutions on amberlite XAD-16 resin, J. Hazard. Mater., 105 (2003) 143–156.
[12] A. Ghaffari, S.M. Tehrani, S.W. Husain, M. Anbia, P.A. Azar, Adsorption of chlorophenols from aqueous solution over amino-modified ordered nanoporous silica materials, J. Nanostruct. Chem., 4 (2014) 1–10.
[13] A. Adewuyi, A. Gopfert, O.A. Adewuyi, T. Wolff, Adsorption of 2-chlorophenolonto the surface of underutilized seed of *Adenopus breviflorus*: a potential means of treating waste water, J. Environ. Chem. Eng., 4 (2016) 664–672.
[14] A.E. Navarro, N.A. Cuizano, R.F. Portales, B.P. Llanos, Adsorptive removal of 2-nitrophenol and 2-chlorophenol by cross- linked Algae from aqueous solutions, Sep. Sci. Technol., 43 (2008) 3183–3199.
[15] M.K. Alam, M.M. Rahman, M. Abbas, S.R. Torati, A.M. Asiri, D. Kim, C.G. Kim, Ultra-sensitive 2-nitrophenol detection based on reduced grapheme oxide/ZnO nanocomposites, J. Electroanal. Chem., 788 (2017) 66–73.

[16] E. Abroushan, S. Farhadi, A. Zabardasti, $Ag_3PO_4/CoFe_2O_4$ magnetic nanocomposite: synthesis, characterization and applications in catalytic reduction of nitrophenols and sunlight-assisted photocatalytic degradation of organic dye pollutants, RSC Adv., 7 (2017) 18293–18304.
[17] E. Bazrafshan, A.H. Mahvi, S. Nasseri, M. Shaieghi, Performance evaluation of electrocoagulation process for diazinon removal from aqueous environments by using iron electrodes, J. Environ. Health Sci. Eng., 4 (2007) 127–132.
[18] A.H. Mahvi, Application of ultrasonic technology for water and wastewater treatment, Iran J. Public Health, 38 (2009) 1–17.
[19] A. Maleki, A.H. Mahvi, A. Mesdaghinia, K. Naddafi, Degradation and toxicity reduction of phenol by ultrasound waves, Bull. Chem. Soc. Ethiop., 21 (2007) 33–38.
[20] A.B. Pandit, P.R. Gogate, S. Mujumdar, Ultrasonic degradation of 2:4:6 trichlorophenol in presence of TiO_2 catalyst, Ultrason. Sonochem., 8 (2001) 227–231.
[21] X. Mao, I.D. Buchanan, S.J. Stanley, Phenol removal from aqueous solution by fungal peroxidises, J. Environ. Eng. Sci., 5 (2006) 103–109.
[22] A.H. Mahvi, A. Maleki, M. Ali Mohamadi, A. Ghasri, Photo-oxidation of phenol in aqueous solution: toxicity of intermediates, Korean J. Chem. Eng., 24 (2007) 79–82.
[23] R.A.D. Tilaki, M.A. Zazooli, J. Yazdani, M.A. Ghaliloo, E. Rostamali, Degradation of 4-chlorophenol by sunlight using catalyst of zinc oxide, J. Mazandaran Univ. Med. Sci., 23 (2014) 196–201.
[24] Y.Q. Wang, B. Gu, W.L. Xu, Electro-catalytic degradation of phenol on several metal oxide anodes, J. Hazard. Mater., 162 (2009) 1159–1164.
[25] M. Li, C. Feng, W. Hu, Z. Zhang, N. Sugiura, Electrochemical degradation of phenol using electrodes of Ti/RuO_2-Pt and Ti/IrO_2-Pt, J. Hazard. Mater., 162 (2009) 455–462.
[26] C. Yang, Y. Qian, L. Zhang, J. Feng, Solvent extraction process development and on- site trial-plant for phenol removal from industrial coal-gasification wastewater, Chem. Eng., 117 (2006) 179–185.
[27] M. Caetano, C. Valderrama, A. Farran, J.L. Cortina, Phenol removal from aqueous solution by adsorption and ion exchange mechanisms onto polymeric resins, J. Colloid Interface Sci., 338 (2009) 402–409.
[28] B. Abussaud, H.A. Asmaly, T.A. Saleh, V.K. Gupta, T. Laoui, M.A. Atieh, Sorption of phenol from water on activated carbon impregnated with iron oxide, aluminum oxide and titanium oxide, J. Mol. Liq., 213 (2016) 351–359.
[29] S.M. Anisuzzaman, A. Bono, D. Krishnaiah, Y.Z. Tan, A study on dynamic simulation of phenol adsorption in activated carbon packed bed column, J. King Saud Univ. Eng. Sci., 28 (2016) 47–55.
[30] S.M. Alshehri, M. Naushad, T. Ahamad, Z.A. Alothman, A. Aldalbahi, Synthesis, characterization of curcumin based ecofriendly antimicrobial bio-adsorbent for the removal of phenol from aqueous medium, Chem. Eng. J., 254 (2014) 181–189.
[31] K. Singh, V.K. Singh, S.K. Verma, R. Bharose, A. Suman, Characterization of modified polypropylene powder (Accurel) and its use for adsorption of phenolics from aqueous solution, Ind. J. Chem. Technol., 20 (2013) 385–391.
[32] K. Singh, S.K. Verma, R. Bharose, Powdered activated mustard cake (PAMC): Synthesis, characterization and its use for aqueous phase adsorption of phenolics, J. Indian Chem. Soc. ICS, 91 (2014) 483–496.
[33] K. Singh, B. Chandra, Adsorption behaviours of phenols onto high specific area activated carbon derived from Trapabispinosa, Ind. J. Chem. Technol., 22 (2015) 11–19.
[34] K. Singh, B. Chandra, Adsorption behaviours of phenols onto modified activated carbon ECH derived from an agriculture waste (Eleusinecoracana husk), Ind. J. Chem. Technol., 92 (2015) 355.
[35] K. Singh, B. Chandra, M. Gautam, Development of inexpensive adsorbent from agro waste for phenol adsorption, JSIR, 75 (2016) 444–451.
[36] A. Kumar, M. Naushad, A. Rana, Inamuddin, Preeti, G. Sharma, A.A. Ghfar, F.J. Stadler, M.R. Khan, ZnSe-WO_3 nano-hetero-assembly stacked on Gum ghatti for photo-degradative removal of Bisphenol A: symbiose of adsorption and photocatalysis, Int. J. Biol. Macromol., 104 (2017) 1172–1184.
[37] P. Dhiman, M. Naushad, K.M. Batoo, A. Kumar, G. Sharma, A.A. Ghfar, G. Kumar, M. Singh, Nano $Fe_xZn_{1-x}O$ as a tuneable and efficient photocatalyst for solar powered degradation of bisphenol A from aqueous environment, J. Clean. Prod., 165 (2017) 1542–1556.
[38] A. Kumar, A. Kumar, G. Sharma, A.H. Al-Muhtaseb, M. Naushad, A.A. Ghfar, C. Guo, F.J. Stadler, Biochar-templated g-$C_3N_4/Bi_2O_2CO_3/CoFe_2O_4$ nano-assembly for visible and solar assisted photo-degradation of paraquat, nitrophenol reduction and CO_2 conversion, Chem. Eng. J., 339 (2018) 393–410.
[39] A.A. Al-Kahtani, T. Almuqati, N. Alhokbany, T. Ahamad, M. Naushad, S.M. Alshehri, A clean approach for the reduction of hazardous 4-nitrophenol using gold nanoparticles decorated multiwalled carbon nanotubes, J. Clean. Prod., 191 (2018) 429–435.
[40] A.M. Peiro, J.A. Ayllón, J. Peral, X. Doménech, TiO_2-photocatalyzed degradation of phenol and ortho-substituted phenolic compounds, Appl. Catal., B, 30 (2001) 359–373.
[41] S. Chen, Z.P. Xu, Q. Zhang, G.Q. Max Lu, Z.P. Hao, S. Liu, Studies on adsorption of phenol and 4-nitrophenol on MgAl-mixed oxide derived from MgAl-layered double hydroxide, Sep. Purif. Technol., 67 (2009) 194–200.
[42] A. Ragavan, A.I. Khan, D.O. Hare, Isomer selective ion-exchange intercalation of nitrophenolates into the layered double hydroxide $[LiAl_2(OH)_6]Cl{\cdot}xH_2O$, J. Mater. Chem., 16 (2006) 602–608.
[43] W. Wang, J. Zhang, F. Chen, D. He, M. Anpo, Preparation and photocatalytic properties of Fe^{3+}-doped Ag@TiO_2 core-shell nanoparticles, J. Colloid Interface Sci., 323 (2008) 182–186.
[44] S.A. Shahid, A. Nafady, I. Ullah, H. Yun, T. Yap, I. Shakir, F. Anwar, U. Rashid, Characterization of newly synthesized $ZrFe_2O_5$ nanomaterial and investigations of its tremendous photocatalytic properties under visible light irradiation, J. Nanomat., 2013 (2013) 1–6.
[45] K.P. Govind Mallan, A. Jain, S. Gayathri, S. Kalainathan, Preparation and magnetic properties of nano size zirconium ferrite particles using co precipitation method, Chem. Technol. Res., 6 (2014) 2187–2189.
[46] X. Dou, G.C. Wang, M. Zhu, F. Liu, W. Li, M. Dinesh, C.U.P. Jr, Identification of Fe and Zr oxide phases in an iron-zirconium binary oxide and arsenate complexes adsorbed onto their surfaces, J. Hazard. Mater., 353 (2018) 1–29.
[47] K. Gupta, K. Biswas, U.C. Ghosh, Nanostructure Fe(III)-Zr(IV) binary mixed oxide: synthesis, characterization, and physicochemical aspects of As(III) sorption from the aqueous solution, J. Ind. Eng. Chem. Res., 4 (2008) 9903–9912.
[48] K. Gupta, T. Basu, U.C. Ghosh, Sorption characteristics of arsenic (v) for removal from water using agglomerated nanostructure Fe(III)-Zr(IV) bimetal mixed oxide, J. Chem. Eng., 54 (2009) 2222–2228.
[49] Z. Ren, G. Zhang, J.P. Chen, Adsorptive removal of arsenic from water by an iron– zirconium binary oxide adsorbent, J. Colloid Interface Sci., 358 (2011) 230–237.
[50] F. Long, J.L. Gong, G. M. Zeng, L. Chen, X.Y. Wang, J.H. Deng, Q.Y. Niu, H.Y. Zhang, X.R. Zhang, Removal of phosphate from aqueous solution by magnetic Fe–Zr binary oxide, Chem. Eng. J., 171 (2011) 448–455.
[51] U. Schwertmann, R.M. Cornell, Iron Oxides in the Laboratory: Preparation and Characterization, second ed., Wiley-VCH, Weinheim, 2000.
[52] A. Hofmann, M. Pelletier, L. Michot, A. Stradner, P. Schurtenberger, R. Kretzschmar, Characterization of the pores in hydrous ferric oxide aggregates formed by freezing and thawing, J. Colloid Interface Sci., 271 (2004) 163–173.
[53] Y. Wang, D. Liu, J. Lu, J. Huang, Enhanced adsorption of hexavalent chromium from aqueous solutions on facilely synthesized mesoporous iron-zirconium bimetal oxide, Colloid Surf., A, 481 (2015) 133–142.

[54] Z. Ren, L. Shao, G. Zhang, Adsorption of phosphate from aqueous solution using an iron–zirconium binary oxide sorbent, Water Air Soil Pollut., 223 (2012) 4221–4231.
[55] M. Naushad, T. Ahamad, B.M. Al-Maswari, A.A. Alqadami, S.M. Alshehri, Nickel ferrite bearing nitrogen-doped mesoporous carbon as efficient adsorbent for the removal of highly toxic metal ion from aqueous medium, Chem. Eng. J., 330 (2017) 1351–1360.
[56] C. Urlacher, J. Mugnier, Waveguide Raman spectroscopy used for structural investigations of ZrO_2 sol-gel waveguiding layers, J. Raman Spectrosc., 27 (1996) 785–792.
[57] Y.S. Li, J.S. Church, A.L. Woodhead, Infrared and Raman spectroscopic studies on iron oxide magnetic nanoparticles and their surface modifications, J. Magn. Magn. Mater., 324 (2012) 1543–1550.
[58] A.A. Alqadami, M. Naushad, Z.A. Alothman, A.A. Ghfar, Novel Metal–Organic Framework (MOF) based composite material for the sequestration of U(VI) and Th(IV) metal ions from aqueous environment, ACS Appl. Mater. Interfaces, 9 (2017) 36026–36037.
[59] K. Singh, M. Gautam, B. Chandra, A. Kumar, Removal of Pb(II) from its aqueous solution by activated carbon derived from Balam Khira (Kigelia Africana), Desal. Wat. Treat., 57 (2016) 1–11.
[60] N.S. Kumar, K. Min, Removal of phenolic compounds from aqueous solutions by biosorption onto *Acacia Leucocephala* bark powder: equilibrium and kinetic studies, J. Chil. Chem. Soc., 56 (2011) 539–545.
[61] B. Zhang, F. Lia, T. Wub, D. Sunb, Y. Lia, Adsorption of p-nitrophenol from aqueous solutions using nanographite oxide, Colloid Surf., A, 464 (2015) 78–88.
[62] M. Masomi, A.A. Ghoreyshi, G.D. Najafpour, A.R. Mohamed, Adsorption of phenolic compounds onto the activated carbon synthesized from pulp and paper mill sludge: equilibrium isotherm, kinetics, thermodynamics and mechanism studies, IJE Trans A Basics, 27 (2014) 1485–1494.
[63] J.M. Li, X.G. Meng, C.W. Hu, J. Du, Adsorption of phenol, p-chlorophenol and p-nitrophenol onto functional chitosan, Bioresour. Technol., 100 (2009) 1168–1173.
[64] K. Singh, M. Gautam, Development of inexpensive biosorbents from de-oiled mustard cake for effective removal of As(V) and Pb(II) ions from their aqueous solutions, J. Environ. Chem. Eng., 5 (2017) 4728–4741.
[65] Y. Liu, Y.J. Liu, Biosortion isotherms, kinetics and thermodynamics, Sep. Purif. Technol., 61 (2008) 229–242.
[66] V. Vimonses, S. Lei, B. Jin, C.W. Chow, C. Saint, Kinetic study and equilibrium isotherm analysis of Congo Red adsorption by clay materials, Chem. Eng. J., 148 (2009) 354–364.
[67] B. Chu, B. Baharin, Y. Che Man, S. Quek, Separation of vitamin E from palm fattyacid distillate using silica: I Equilibrium of batch adsorption, J. Food Eng., 62 (2004) 97–103.
[68] Y. Ho, G. McKay, Comparative sorption kinetic studies of dye and aromatic compounds onto fly ash, J. Environ. Sci. Health A, 34 (1999) 1179–1204.
[69] N.G.R. Silva, J.C.M. Pirajan, L.G. Giraldo, Thermodynamic study of adsorption of phenol, 4-chlorophenol and 4-nitrophenol on activated carbon obtained from eucalyptus seed, J. Chem., 2015 (2015) 1–9.
[70] M. Ahmaruzzaman, S.L. Gayatri, Activated neem leaf: a novel adsorbent for the removal of phenol, 4-nitrophenol and 4-chlorophenol from aqueous solutions, J. Chem. Eng. Data, 56 (2011) 3004–3016.
[71] U. Thawornchaisit, K. Pakulanon, Application of dried sewage sludge as phenol biosorbent, Bioresour. Technol., 98 (2007) 140–144.
[72] Z. Aksu, J. Yener, Investigation of the biosorption of phenol and monochlorinated phenols on the dried activated sludge, J. Process Biochem., 33 (1998) 649–655.
[73] M. Otero, F. Rozada, L.F. Calvo, A.I. Garca, A. Moran, Elimination of organic water pollutants using adsorbents obtained from sewage sludge, Dyes Pigm., 57 (2003) 55–65.
[74] H. Polat, M. Molva, M. Polat, Capacity and mechanism of phenol adsorption on lignite, Int. J. Miner. Process, 79 (2006) 264–273.
[75] Z. Aksu, J. Yener, A comparative adsorption/biosorption study of mono-chlorinated phenols onto various sorbents, Waste Manage., 21 (2001) 695–702.
[76] C. Xiaoli, Z. Youcai, Adsorption of phenolic compound by aged-refuse, J. Hazard. Mater., B137 (2006) 410–417.
[77] E. Rubín, P. Rodrígue, R, Herrero, de V. Sastre, E. Manuel, Biosorption of phenolic compounds by the brown alga Sargassum muticum, J. Chem. Technol. Biotechnol., 81 (2006) 1093–1099.
[78] V.K. Gupta, I. Ali, V.K. Saini, Removal of chlorophenols from wastewater using red mud: an aluminium industry waste, Environ. Sci. Technol., 38 (2004) 4012–4018.
[79] L.C. Zhou, X. G. Meng, J.W. Fu, Y.C. Yang, P. Yang, C. Mi, Highly efficient adsorption of chlorophenols onto chemically modified chitosan, Appl. Surf. Sci., 292 (2014) 735–741.
[80] B.K. Singh, P.S. Nayak, Sorption equilibrium studies of toxic nitro-substituted phenols on fly ash, Adsorpt. Sci. Technol., 22 (2004) 295–310.
[81] A.E.H. Daifullah, H. Gad, Sorption of semi-volatile organic compounds by bottom and fly ashes using HPLC, Adsorpt. Sci. Technol., 16 (1998) 273–283.

Supplementary information:

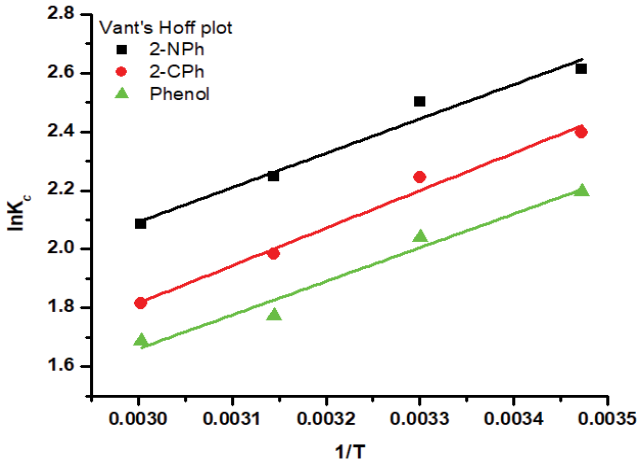

Fig. S1. Van't Hoff plot for the adsorption of phenol, 2-chlorophenol and 2-nitrophenol on zirconium-ferrite nanoparticles.

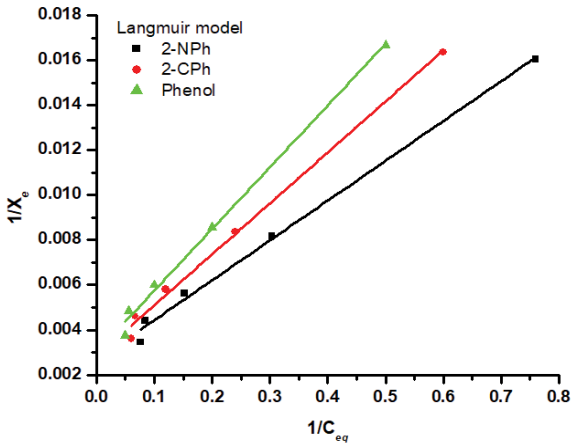

Fig. S2. Langmuir adsorption isotherm for the adsorption of phenol, 2-chlorophenol and 2-nitrophenol on zirconium-ferrite nanoparticles at 288 K.

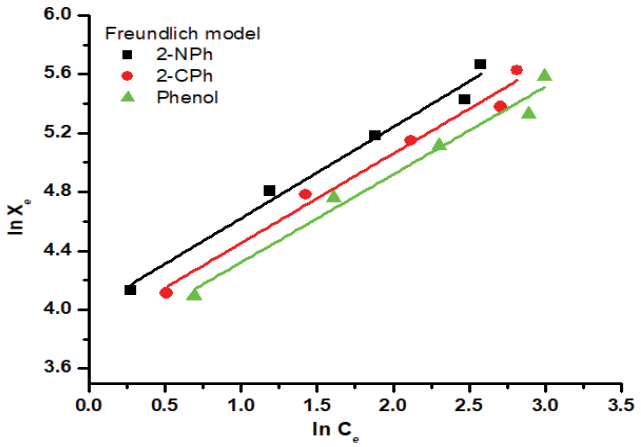

Fig. S3. Freundlich adsorption isotherm for the adsorption of phenol, 2-chlorophenol and 2-nitrophenol on zirconium-ferrite nanoparticles at 288 K.

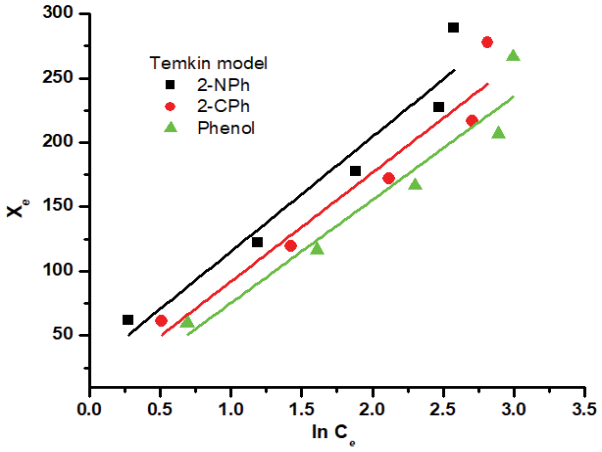

Fig. S4. Temkin adsorption isotherm for the adsorption of phenol, 2-chlorophenol and 2-nitrophenol on zirconium-ferrite nanoparticles at 288 K.

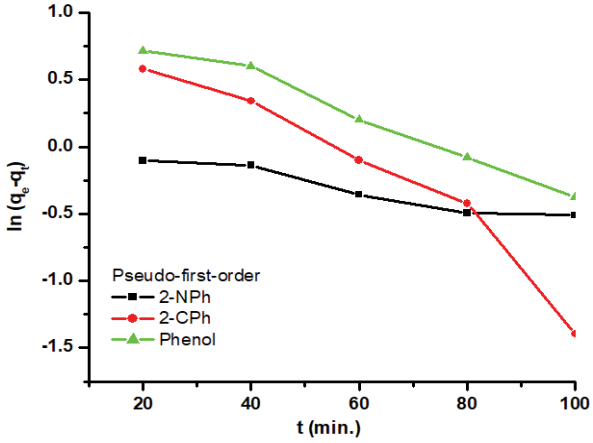

Fig. S5. Pseudo-first-order kinetic model for the adsorption of phenol, 2-chlorophenol and 2-nitrophenol on zirconium-ferrite nanoparticles.

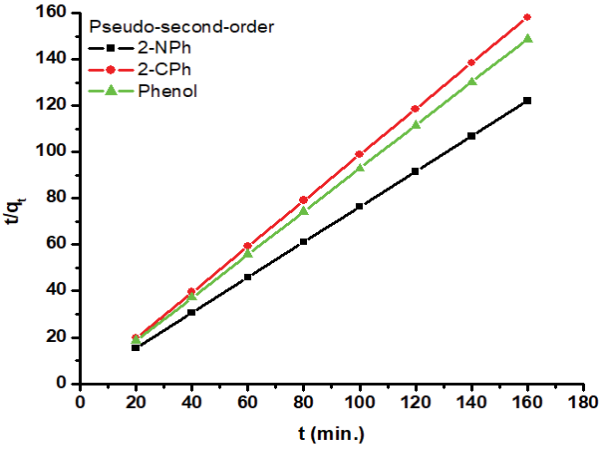

Fig. S6. Pseudo-second-order kinetic model for the adsorption of Phenol, 2-Chlorophenol and 2-nitrophenol on zirconium-ferrite nanoparticles